Comparative analysis of $Fe_3O_4/CoFe_2O_4$ and $NiZnFe_2O_4/MnZnFe_2O_4$ hybrid ferro-nanofluids flow under magnetic dipole effect over a slip stretching sheet

Nur Ilyana Kamis, Lim Yeou Jiann, Sharidan Shafie, Noraihan Afiqah Rawi [*]

Department of Mathematical Sciences, Faculty of Science, Universiti Teknologi Malaysia, 81310, Johor Bahru, Johor, Malaysia

ARTICLE INFO

ABSTRACT

The available external manipulation of ferrofluids through magnetic fields leads to applications in magnetically controlled actuation and drug targeting. This study investigates the behavior of magnetic hybrid ferro-nanofluids flowing over a stretched sheet with the inclusion of velocity slip and a magnetic dipole. The thermal characteristic of two different hybrid ferro-nanofluids, which are ferrite-cobalt ferrite ($Fe_3O_4/CoFe_2O_4$) and nickel zinc ferrite-manganese zinc ferrite ($NiZnFe_2O_4/MnZnFe_2O_4$) dispersed into a water-ethylene glycol, are theoretically analyzed and compared. The governing equations are developed using the Tiwari and Das model. The simplified equations are solved using the Keller box method. Results show that increased ferro-hydrodynamic interaction and slip velocity contribute to higher velocity profiles. A stronger magnetic field intensity, by increasing the distance of the magnetic dipole, significantly improves the velocity profile but leads to a rapid decline in the temperature field. It is found that as the dimensionless distance increases, the temperature profile drops 0.15 % from $Fe_3O_4/CoFe_2O_4$ to $NiZnFe_2O_4/MnZnFe_2O_4$. There is an immediate 0.45 % drop in the velocity profile for $Fe_3O_4/CoFe_2O_4$ as velocity slip enhances, compared to $NiZnFe_2O_4/MnZnFe_2O_4$. The thermal field rises by 1.93 % as the magnetic field distance approaches the plate, influenced by the hybrid nano-particles' volume fraction.

Nomenclature

U_w	stretching velocity
T_w	sheet temperature
T_∞	ambient or bulk temperature
T_c	Curie temperature
(u, v)	velocity components for (x, y)
ρ	density
μ	dynamic viscosity
ρC_p	heat capacity
k	thermal conductivity

T	temperature
M	magnetization
H	magnetic field
g	gravitational acceleration
β^*	thermal expansion
α^*	inclination angle
d	distance of the magnetic dipole
K	thermomagnetic
Pr	Prandtl number
ε	Curie temperature
χ	viscous dissipation
β	ferrohydrodynamic interaction parameter
δ	Velocity slip
α	dimensionless distance
Re_x	Reynold number
C_f	local skin friction
Nu_x	Nusselt number
τ_w	wall shear stress
q_w	heat transfer rate

1. Introduction

Engineering, physics, and environmental sciences all heavily depend on heat transfer, a fundamental phenomenon that occurs in various systems. Due to its numerous applications, such as heat exchange, pharmaceuticals, and biotechnology, the study of heat transfer in fluids is of utmost importance. Steve Papell [1] invented a new type of fluid called ferrofluid in 1963. The primary objective in developing this fluid was to propel liquid fuel in a rocket within a zero-gravity environment using a magnetic field. According to Rosensweig [2], ferrofluid is a magnetic nanoparticle in the form of a colloidal solution, with the size of the iron oxide particles used during manufacturing being approximately 10 nm. To prevent their agglomeration and stabilise the suspension, the magnetic nanoparticles are coated with a surfactant and suspended in a liquid carrier. It is worth mentioning that the thermal conductivity of ferrofluid is relatively low [3], and the magnetization of magnetic nanoparticles and temperature gradient affect convection within the ferrofluid [4]. Furthermore, the thermal conductivity of ferrofluid is determined by the strength of the magnetic field imposed on it [5, 6]. Unlike typical non-magnetic nanofluids, magnetic nanoparticles offer several advantages, including higher saturation magnetization and cost-effectiveness [7]. Therefore, Andersson and Valnes [8] initially explored the heat transfer of ferrofluid in the presence of a magnetic field. Through this study, the effects of ferrohydrodynamic (FHD) effects on the heat transfer of a ferrofluid were studied. FHD refers to the study of magnetic fluid motion due to magnetic polarisation forces. They investigated the magneto-thermomechanical effect, involving the coupling of ferrohydromagnetic momentum and thermal energy equations. When a magnetic field is applied to ferrofluid, the suspended magnetic nanoparticles become magnetised and align themselves with the field, resulting in changes in the fluid's properties [2,9].

After the introduction of the nanofluid concept by Choi and Eastman [10], some researchers adopted ferrofluid as ferro-nanofluid due to the enhanced thermal conductivity resulting from a small percentage of magnetic nanoparticles [11]. Subsequently, researchers began exploring ferro-nanofluids by adopting the nanofluid model. For example, Muhammad and Nadeem [12] three different magnetic nanoparticles dissolved in ethylene glycol (EG). These were nickel-zinc ferrite ($NiZnFe_2O_4$), ferrite (Fe_3O_4), and manganese-zinc ferrite ($MnZnFe_2O_4$). The study claimed that increasing the concentration of ferro nanoparticles up to 20 % decreases the velocity profile but increases the thermal contribution. Muhammad et al. [13] extended this work [12] by considering two types of base fluids, namely EG and water, for $NiZnFe_2O_4$, Fe_3O_4 and $MnZnFe_2O_4$ with Newtonian heating. It was observed that, in contrast to EG, ferro nanoparticles in water exhibit a rapid drop in fluid velocity due to different Prandtl numbers. The findings of [12,13] motivated Nadeem et al. [14] to explore ferro nanoparticles ($NiZnFe_2O_4$, Fe_3O_4 and $MnZnFe_2O_4$) in water. They observed that heat transfer increases with a higher concentration of ferro nanoparticles in the base fluid. The lower density of Fe_3O_4 causes significant

Table 1
Previous studies on hybrid ferro-nanofluid.

Articles	Hybrid ferro-nanofluid	Magnetic field
[18]	$NiZnFe_2O_4/MnZnFe_2O_4$-EG	MHD
[19]	$NiZnFe_2O_4/MnZnFe_2O_4$- kerosene and engine oil	FHD
[20]	$NiZnFe_2O_4/MnZnFe_2O_4$-water	–
[21]	Fe_3O_4 and $MnZnFe_2O_4$-water and refrigerant-134 A ($C_2H_2F_4$)	FHD
[22]	$Fe_3O_4/CoFe_3O_4$- engine oil	FHD
[23]	$Fe_3O_4/CoFe_3O_4$-water	MHD
[24–28]	$Fe_3O_4/CoFe_3O_4$-water plus EG	MHD

velocity changes compared to $CoFe_3O_4$ and $MnZnFe_2O_4$ [15]. Yasin et al. [16] investigated the characteristics of Fe_3O_4 with the magnetohydrodynamic (MHD) effect using the Keller box method. The Nusselt number of Fe_3O_4 was found to be higher than that of $MnZnFe_2O_4$ and $CoFe_3O_4$ in water as the MHD effect increased along with the permeable flat plate [17].

In recent times, the utilisation of two types of magnetic nanoparticles, known as "hybrid ferro-nanofluid," has attracted attention from diverse industries interested in exploring their profound applications in technical, industrial, and scientific domains. Particularly in the field of biomedical engineering, including cancer treatment, magnetic resonance imaging (MRI), and drug delivery, there is considerable interest in further investigating this hybrid ferro-nanofluid. To ascertain the originality of this researcher's work, Table 1 is presented, and the primary conclusion is elucidated.

As a result, an upward trend in magnetic field intensity diminishes the velocity of hybrid ferro-nanofluids, whereas the temperature and concentration of the liquids show the opposite tendency [18]. Moreover, the rate of heat and mass transmission drops in Cu/Al_2O_3 compared to $NiZnFe_2O_4/MnZnFe_2O_4$ as the ferromagnetic interaction parameter improves. Tahir et al. [19] concluded that two or more ferrite nanoparticles suspended in two or more base fluids could enhance the heat transmission of the fluid. An increase in the volume fractions of nanoparticles leads to elevated velocity and temperature gradients as the thickness of the corresponding boundary layer grows [20]. The enhancement of magnetization in $Fe_3O_4/MnZnFe_2O_4$ had a greater impact on the increase of ferrohydrodynamic effects in water compared to $C_2H_2F_4$ [21]. Furthermore, the utilisation of a hybrid ferro-nanofluid has shown significant advantages in terms of heat transfer rate [22]. In comparison to hybrid nanofluid, the flow behavior of hybrid ferro-nanofluid can be more easily controlled through electromagnetic induction. Other than that, researchers also explored the MHD effect for hybrid ferro-nanofluids, $Fe_3O_4/CoFe_3O_4$, in various geometries. For example, Anuar et al. [23] claimed that the escalation of the hybrid ferro-nanofluid boosts the shear stress and heat transfer rate. The hybrid ferrofluid $Fe_3O_4/CoFe_3O_4$ in the combination of EG with water is more impactful in terms of heat transfer than the ferrofluid [24]. The heat transfer rate in hybrid ferro-nanofluids embedded with $CoFe_3O_4$ is higher than that in water and ferrofluids [25]. Then, $Fe_3O_4/CoFe_3O_4$ in a mixture of water and EG due to the rotating disk [26], spinning cone [27], and thin film stretching sheet [28] also affected the pattern of the boundary layer flow.

The alignment of magnetic nanoparticles when exposed to a magnetic field gives rise to distinct flow phenomena, allowing for various applications such as magnetically controlled actuation and enhanced heat transfer. A bar magnet is one type of source that produces a magnetic field. The magnetic bar is commonly known to have two poles, namely the north and south poles. Cullity and Graham [29] utilise magnetic dipoles in fluids with magnetic particles to activate the FHD effect. This is critical for fluid movement. A short magnetic spherical bar generates a larger magnetic field due to its tighter dipole spacing, which in turn generates a stronger magnetic field [30]. An analytical solution by Neuringer and Rosensweig [31] that takes into account magneto-mechanical and thermomagnetic effects demonstrates that an abundance of ferrofluid in a magnetic field encourages the FHD effect. The thermal energy of the ferrofluid escalates under the effect of FHD. Based on the theoretical study reported by Ref. [4], the ferrofluid becomes saturated as the magnetic dipole-induced magnetic field intensity rises. Consequently, the heat transfer rate of ferrofluid decays as the FHD effect rises; however, it increases the shear stress when the sheet is stretched. The rapid reduction of shear stress has been found in the presence of the effect [12–14]. Tabassam et al. [32] claimed that the velocity of the ferrofluid escalates due to the reduction in magnetic field intensity when raising the dimensionless distance of the magnetic dipole. The magnetic dipole reduces the velocity profile, whereas it enhances the thermal energy in the fluid [33,34].

Boundary slip liquids are used in a variety of technological challenges, including the polishing of mechanical heart valves and internal cavities. Andersson [35] and Wang [36] conducted the earlier in-depth study on a slip boundary condition over a stretching sheet. The studies reported an exact solution of the full Navier-Stokes equation due to the stretching sheet embedded with velocity slip. The velocity of fluid flow reduces due to the upsurge of the slip factor. The shear stress of the fluid is found to be diminished. At the same time, the velocity is enhanced by the MHD and suction, as well as the injection effects [37]. The slip factor has a prominent effect on temperature and concentration [38]. Table 2 is provided to show the previous studies on the first-order velocity slip under the impact of FHD [39–43] and MHD [44].

Based on the author's knowledge and understanding of the existing literature, including Tables 1 and 2, no prior studies have investigated the influence of magnetic dipoles and velocity slip on a stretching sheet for hybrid ferro-nanofluids, $Fe_3O_4/CoFe_3O_4$ and $NiZnFe_2O_4/MnZnFe_2O_4$. Therefore, this study aims to fill this research gap by examining and comparing these two hybrid ferro-nanofluids in combination with EG and water, taking into account the slip velocity effect on a stretching sheet. Also, the effect of the magnetic dipole with Curie temperature, the dimensionless distance of the magnetic dipole, and viscous dissipation on the flow of

Table 2
Previous studies on fluid with first-order slip.

Articles	Fluid	Conclusion
[39]	Ferrofluid	Temperature increases as velocity slip increases in ferrofluid with the magnetic dipole.
[40]	Ferro-nanofluid (Buongiorno model)	The velocity profile demonstrates a similar pattern as [35,36].
[41]	Ferro-nanofluid (Tiwari and Das model)	Ferrimagnetic nanoparticles exhibit lower skin friction than anti-ferromagnetic, ferromagnetic, diamagnetic, and paramagnetic nanoparticles while experiencing higher velocity slips.
[42]		The presence of velocity slip contributes to an augmentation in skin friction at the wall, particularly with the escalation of the ferromagnetic interaction parameter.
[43]		The thermal profile in the $Fe_3O_4 - C_2H_2F_4$ nanofluid is detected to elevate due to the reaction of the magnetic dipole and first-order velocity slip.
[44]	Hybrid ferro-nanofluid	When the slip velocity parameter is raised, the slip velocity of the $Cu - Fe_3O_4/EG$ reduces the liquid velocity.

the fluid are studied. The governing equations, which are developed based on previous studies [19,39], are initially in the form of partial differential equations (PDEs). In order to simplify the complexity of the PDEs, we employed suitable similarity equations, which transformed them into ordinary differential equations (ODEs). Subsequently, we utilized the Keller box method to solve these transformed equations. The results are displayed as graphs and tables, providing insights into the velocity and temperature fields as well as physical quantities such as the Nusselt number and local skin friction.

2. Mathematical formulation

In this study, the fluid flow is characterized as steady, incompressible, and laminar, with a two-dimensional Newtonian fluid that exhibits ferromagnetic properties. To simplify the problem, the boundary layer approximation is utilized. The ferromagnetic effect is modelled through the magnetic dipole, and the fluid flow is subjected to a stretching sheet. $U_w = cx$, where c is a constant that denotes the velocity at which the sheet stretches along the x-axis. The y-axis is perpendicular to the sheet. Fig. 1 illustrates the placement of the magnetic dipole beneath the sheet, with its center located on the y-axis at a distance of d [14]. The ferrofluid is restricted to the sheet's positive half-space along the y-axis. The magnetic dipole elevates the magnetic force and leads to saturation in the ferrofluid by generating a magnetic field that is perpendicular to the x-axis. Furthermore, the temperature of the sheet, denoted as T_w, is maintained at a constant value. In contrast, the temperature of the surrounding fluid or bulk fluid, referred to as T_∞, as discussed by Das et al. [40], represents the ambient fluid temperature. The Curie temperature, T_c, signifies the temperature at which the ferromagnetic element loses its magnetism and transitions to a paramagnetic state. In this particular scenario, T_c is equivalent to T_∞. Hybrid ferro-nanofluids are created by suspending mixtures of two types of nanoparticles in the base fluid. The governing equations, including continuity, momentum, and energy equations, are derived by modifying the Tiwari and Das model [25] and can be written as [19]

$$\frac{\partial u}{\partial x} + \frac{\partial v}{\partial y} = 0, \tag{1}$$

$$\rho_{hnf}\left(v\frac{\partial u}{\partial y} + u\frac{\partial u}{\partial x}\right) = M\mu_0\frac{\partial H}{\partial x} + \mu_{hnf}\left(\frac{\partial^2 u}{\partial y^2} + \frac{\partial^2 u}{\partial x^2}\right), \tag{2}$$

$$(\rho C_p)_{hnf}\left(v\frac{\partial T}{\partial y} + u\frac{\partial T}{\partial x}\right) + \left(v\frac{\partial H}{\partial y} + u\frac{\partial H}{\partial x}\right)\mu_0 T\frac{\partial M}{\partial T} = k_{hnf}\left(\frac{\partial^2 T}{\partial y^2} + \frac{\partial^2 T}{\partial x^2}\right) - \mu_{hnf}\left(2\left(\frac{\partial u}{\partial x}\right)^2 + 2\left(\frac{\partial v}{\partial y}\right)^2 + \left(\frac{\partial u}{\partial y} + \frac{\partial v}{\partial y}\right)^2\right) \tag{3}$$

Moreover, the interaction between the fluid and the plate surface is accounted for by incorporating slip boundary conditions [19,39]

$$\text{at } y = 0 : u = U_w + A\frac{\partial u}{\partial y}, v = 0, T = T_w, \tag{4}$$

$$\text{at } y \to \infty : u = 0, T = T_c, \tag{5}$$

The governing equations involve the velocity components (u, v) for the (x, y) directions. The variables $A, k, \rho C_p, \mu,$ and ρ represent the velocity slip factor, thermal conductivity, heat capacity, dynamic viscosity, and density, respectively. The subscript "hnf" denotes the hybrid nanofluid, while μ_0 represents the magnetic permeability. T stands for temperature, and M, and H denote the magnetization
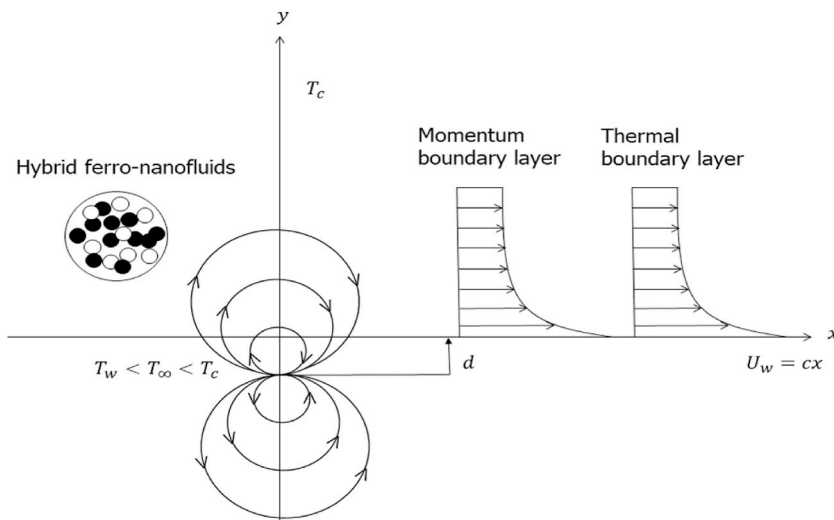
Fig. 1. Physical geometry.

and magnetic field, respectively. The term $M\mu_0\frac{\partial H}{\partial x}$ demonstrates the components of magnetization force, also known as Kelvin force [39]. The second term on the left-hand side of equation (3) represents the heating because of adiabatic magnetization in ferrofluid [39]. The last term in the energy equation (3) is viscous dissipation, which is a heat source induced by fluid particle friction.

2.1. Magnetic dipole

The creation of a magnetic field as a result of the magnetic dipole affects how the ferrofluid flow behaves. The following is an expression for the magnetic scalar potential [19]:

$$\delta = \frac{\gamma_1}{2\pi}\frac{x}{x^2 + (y+d)^2}, \tag{6}$$

The magnetic field strength (H) at the source is represented by γ_1. The components of H can be expressed in the following manner [39]:

$$\frac{\partial H}{\partial x} = -\frac{\partial \delta}{\partial x} = \frac{\gamma_1}{2\pi}\frac{x^2 - (y+d)^2}{\left(x^2 + (y+d)^2\right)^2}, \tag{7}$$

$$\frac{\partial H}{\partial y} = -\frac{\partial \delta}{\partial y} = \frac{\gamma_1}{2\pi}\frac{2x(y+d)}{\left(x^2 + (y+d)^2\right)^2}, \tag{8}$$

since the magnetic body force is directly related to the gradient of H, we can express H as the $\sqrt{\left(\frac{\partial \delta}{\partial y}\right)^2 + \left(\frac{\partial \delta}{\partial x}\right)^2}$. The components of H can be expressed as follows by extending equations (7) and (8) in powers of x and taking into consideration terms up to second order (x^2) [39], we have

$$\frac{\partial H}{\partial x} = -\frac{\gamma_1}{2\pi}\frac{2x}{(y+d)^2}, \tag{9}$$

$$\frac{\partial H}{\partial y} = \frac{\gamma_1}{2\pi}\left(-\frac{2}{(y+d)^3} + \frac{4x^2}{(y+d)^5}\right). \tag{10}$$

The relationship between magnetization (M) and temperature (T) can be expressed as a linear equation [19,39]

$$M = -K(T_c - T), \tag{11}$$

The coefficient K represents the thermomagnetic effect resulting from the thermal gradient on materials' magnetic. For ferrohydrodynamic interaction to occur, two conditions must be met:

i. The fluid must have a temperature T that differs from the Curie temperature T_c,
ii. An inhomogeneous magnetic field must be applied.

The magnetization of the magnetic material in the ferrofluid diminishes once it reaches the Curie temperature. This characteristic holds great importance in various practical operations, primarily because of the considerably huge Curie temperature exhibited by iron, which is approximately 1043 K.

2.2. Dimensionless equation

Equations (1)–(5) are expressed as PDEs. To simplify these equations, the similarity transformations are employed, which lead to a reduced set of ODEs [19].

$$\psi(\xi,\eta) = \left(\frac{\nu}{\rho}\right)^{\frac{1}{2}}\xi f(\eta), \eta = \left(\frac{c\rho}{\mu}\right)^{\frac{1}{2}}y, \xi = \left(\frac{c\rho}{\mu}\right)^{\frac{1}{2}}x, \theta(\xi,\eta) = \frac{T_c - T}{T_c - T_w} = \theta_1(\eta) + \xi^2\theta_2(\eta), \tag{12}$$

Here, $\theta(\xi,\eta)$ indicates the dimensionless temperature with the similarity variables (ξ,η). $\psi(x,y)$ is stream function that can be expressed as $u = \frac{\partial \psi}{\partial y} = cxf'(\eta)$ and $v = -\frac{\partial \psi}{\partial x} = -(c\mu/\rho)^{\frac{1}{2}}f(\eta)$. These equations ensure the satisfaction of the continuity equation (1). Equation (12) is substituted into equation (2) to (3) to provide the following result:

$$\left(\frac{\mu_{hnf}}{\mu_{bf}}\right)f''' - f'^2 + ff'' - \frac{2\left(\mu_{bf}/\mu_{hnf}\right)\beta\theta_1}{(\eta+\alpha)^4} = 0, \tag{13}$$

$$\left(\frac{k_{hnf}}{k_{bf}}\right)(\theta_1'' + 2\theta_2) + \left(\frac{(\rho C_p)_{hnf}}{(\rho C_p)_{bf}}\right)Pr\,\theta_1'f + \frac{2\chi\beta f(\theta_1 - \varepsilon)}{(\eta+\alpha)^3} - \left(\frac{\mu_{hnf}}{\mu_{bf}}\right)4\chi f'^2 = 0, \tag{14}$$

$$\left(\frac{k_{hnf}}{k_{bf}}\right)\theta_2'' - \left(\frac{(\rho C_p)_{hnf}}{(\rho C_p)_{bf}}\right)Pr\left(2f'\theta_2 - f\theta_2'\right) + \frac{2\chi\beta f\theta_2}{(\eta+\alpha)^3} - \lambda\beta(\theta_1-\varepsilon)\left[\frac{2f'}{(\eta+\alpha)^4} + \frac{4f}{(\eta+\alpha)^5}\right] - \left(\frac{\mu_{hnf}}{\mu_{bf}}\right)\chi f''^2 = 0, \tag{15}$$

The boundary conditions (4) and (5) can be simplified to the following:

$$\text{at } \eta = 0 : f(\eta) = 0, f'(\eta) = 1 + \delta f''(\eta), \theta_1(\eta) = 1, \theta_2(\eta) = 0, \tag{16}$$

$$\text{at } \eta \to \infty : f'(\eta) \to 0, \theta_1(\eta) \to 0, \theta_2(\eta) \to 0. \tag{17}$$

where the dimensionless Curie temperature (ε), Prandtl number (Pr), dimensionless distance (α), ferrohydrodynamic interaction (β), viscous dissipation (χ), and velocity slip (δ). These parameters are defined as

$$\varepsilon = \frac{T_\infty}{T_c - T_w}, Pr = \frac{\nu}{\alpha}, \alpha = \sqrt{\frac{c\rho d^2}{\mu}}, \beta = \frac{\gamma}{2\pi}\frac{\mu_0 K(T_c - T_w)\rho}{\mu^2}, \chi = \frac{c\mu^2}{\rho k(T_c - T_w)}, \delta = A\left(\frac{c\rho}{\mu}\right)^{\frac{1}{2}} \tag{18}$$

According to Refs. [26–28], the utilized base fluid in the formulation of the Newtonian hybrid ferro-nanofluid is a mixture of water with EG. Due to its Newtonian behavior, in which its viscosity stays constant as the shear rate increases [45]. Spherical-shaped magnetic nanoparticles, including Fe_3O_4, $CoFe_2O_4$, $NiZnFe_2O_4$ and $MnZnFe_2O_4$ are dissolved into the base fluid. The use of spherical particles is advantageous as they have a high surface area-to-volume ratio. The smaller magnetic nanoparticles exhibit traits including low sedimentation rates and energy levels. Based on an experimental study by Elsayed et al. [46], magnetic nanocomposites are synthesized by the in situ precipitation method. Spinel cubic structures for ferrite nanoparticles were reported after X-ray diffraction analysis (XRD). Moreover, magnetic nanoparticles have a large specific surface area and high magnetization based on the transmission electron microscopy test (TEM) [47]. The thermophysical properties of the base fluid and nanoparticles at a temperature of 25 °C are comprehensively summarized in Table 3 [48]. Table 4 provides the modification of the Tiwari and Das model of the hybrid ferro-nanofluids. In the tables, the superscripts s_1, s_2, nhf, bf, φ_1, and φ_2 represent the first and second solid nanoparticles, hybrid ferro-nanofluid, base fluid, and first and second nanoparticle volume fractions, respectively. This study considers two set of hybrid ferro-nanoparticles which are $(Fe_3O_4(s_1\varphi_1)/CoFe_2O_4\ (s_2\varphi_2))_1$ and $(NiZnFe_2O_4(s_1\varphi_1)/MnZnFe_2O_4(s_2\varphi_2))_2$, respectively.

2.3. Physical quantities

The local skin friction, denoted as C_f, and Nusselt number, represented as Nu_x, can be defined as follows [39]:

$$C_f = -\frac{2\tau_w}{\rho_{bf}U_w^2},$$

and

$$Nu_x = \frac{xq_w}{k_{bf}(T_c - T_w)}, \tag{19}$$

here, $\tau_w(x)$ refers to wall shear stress and $q_w(x)$ is heat transfer rate that can be described as

$$\tau_w = \mu_{hnf}\frac{\partial u}{\partial y}\bigg|_{y=0}$$

and

Table 3
The thermophysical characteristics of the base fluid and magnetic nanoparticles [19,25,27].

Properties	Ethylene glycol (EG) (50 %) plus water (50 %)	Fe_3O_4	$CoFe_2O_4$	$NiZnFe_2O_4$	$MnZnFe_2O_4$
$\rho(kgm^{-3})$	1056	5180	4907	4800	4700
$C_p(Jkg^{-1}K^{-1})$	3.288	670	700	710	1050
$k(Wm^{-1}K^{-1})$	0.425	9.7	3.7	6.3	3.9
Pr	29.86	–	–	–	–

Table 4

Modification of Tiwari and Das model [25,28].

Properties	Hybrid ferro-nanofluids
Viscosity	$\mu_{hnf} = \dfrac{\mu_{bf}}{(1-\varphi_{1i})^{2.5}(1-\varphi_{2i})^{2.5}}$
Density	$\rho_{hnf} = (1-\varphi_{2i})[(1-\varphi_{1i})\rho_{bf} + \varphi_{1i}\rho_{s_{1i}}] + \varphi_{2i}\rho_{s_{2i}}$
Specific heat capacity	$(\rho C_p)_{hnf} = (1-\varphi_{2i})[(1-\varphi_{1i})(\rho C_p)_{bf} + \varphi_{1i}(\rho C_p)_{s_{1i}}] + \varphi_{2i}(\rho C_p)_{s_{2i}}$
Thermal conductivity	$k_{hnf} = \dfrac{k_{s_{2i}} + 2k_{nf} - 2\varphi_{2i}(k_{nf} - k_{s_{2i}})}{k_{s_{2i}} + 2k_{nf} + \varphi_{2i}(k_{nf} - k_{s_{2i}})} \times k_{nf}$
	where
	$\dfrac{k_{nf}}{k_{bf}} = \dfrac{k_{s_{1i}} + 2k_{bf} - 2\varphi_{2i}(k_{bf} - k_{s_{1i}})}{k_{s_{1i}} + 2k_{bf} + \varphi_{2i}(k_{bf} - k_{s_{1i}})}$

$i = 1$ for the first set of hybrid ferro-nanofluids (Fe_3O_4 /$CoFe_2O_4$).

$i = 2$ for the second set of hybrid ferro-nanofluids ($NiZnFe_2O_4$ /$MnZnFe_2O_4$).

$$q_w = -k_{hnf}\frac{\partial T}{\partial y}\bigg|_{y=0}. \tag{20}$$

By utilizing equation (12), we can express the dimensionless C_f and Nu_x coefficients as follows [19,39]

$$C_f Re_x^{\frac{1}{2}} = -\frac{2}{\mu_{hnf}}f''(0)$$

and

$$Re_x^{-\frac{1}{2}}Nu_x = -\frac{k_{hnf}}{k_{bf}}\left[\theta_1'(0) + \xi^2\theta_2'(0)\right]. \tag{21}$$

3. Numerical approach

The Keller box strategy is utilized. The governing equations (13) to (15) and boundary conditions (16) to (17) are resolved. The Keller box approach is a numerical technique used for solving partial differential equations. It involves discretizing the domain into a grid and approximating the solution at each grid point. This method is particularly accurate for nonlinear problems. It is worth highlighting that this numerical scheme is easier to use, more adaptable, and more effective compared to other numerical methods like the local nonsimilarity method. It provides highly accurate numerical results. Additionally, the method is numerically stable, allowing for reliable computations [49]. Following the four primary steps as shown below and the computational methods outlined in Fig. 2 leads to a numerical solution.

i. $f = f, f' = u, f'' = v, \theta_1 = \theta, \theta_1' = s, \theta_2 = g, \theta_2' = w$ are the new dependent variables that have been introduced to reduce the governing equations into a first-order system such as

$$\left(\frac{\mu_{hnf}}{\mu_{bf}}\right)v' - u^2 + fv - \frac{2\left(\mu_{bf}/\mu_{hnf}\right)\beta\theta}{(\eta+\alpha)^4} = 0, \tag{22}$$

$$\left(\frac{k_{hnf}}{k_{bf}}\right)(s'+2g) + \left(\frac{(\rho C_p)_{hnf}}{(\rho C_p)_{bf}}\right)Prsf + \frac{2\chi\beta f(\theta-\varepsilon)}{(\eta+\alpha)^3} - \left(\frac{\mu_{hnf}}{\mu_{bf}}\right)4\chi u^2 = 0, \tag{23}$$

$$\left(\frac{k_{hnf}}{k_{bf}}\right)w' - \left(\frac{(\rho C_p)_{hnf}}{(\rho C_p)_{bf}}\right)Pr(2ug - fw) + \frac{2\chi\beta fg}{(\eta+\alpha)^3} - \lambda\beta(\theta-\varepsilon)\left[\frac{2u}{(\eta+\alpha)^4} + \frac{4f}{(\eta+\alpha)^5}\right] - \left(\frac{\mu_{hnf}}{\mu_{bf}}\right)\chi v^2 = 0 \tag{24}$$

ii. The technique known as the finite difference is used for the first-order derivatives outlined in the preceding section. The central difference approach is used to approximate equations (22) to (24).

START

PRE-PROCESS
(Computing the independent variables, step size, etc.)

Initializing
$k = 1$

Computes the initial profile of the interested physical
variables

Computes the elements of matrix

Generates the coefficients of the finite difference

Solve the linear system using block elimination

$|\delta v_0|$
$< 1 \times 10^{-5}$?

NO

YES

STOP
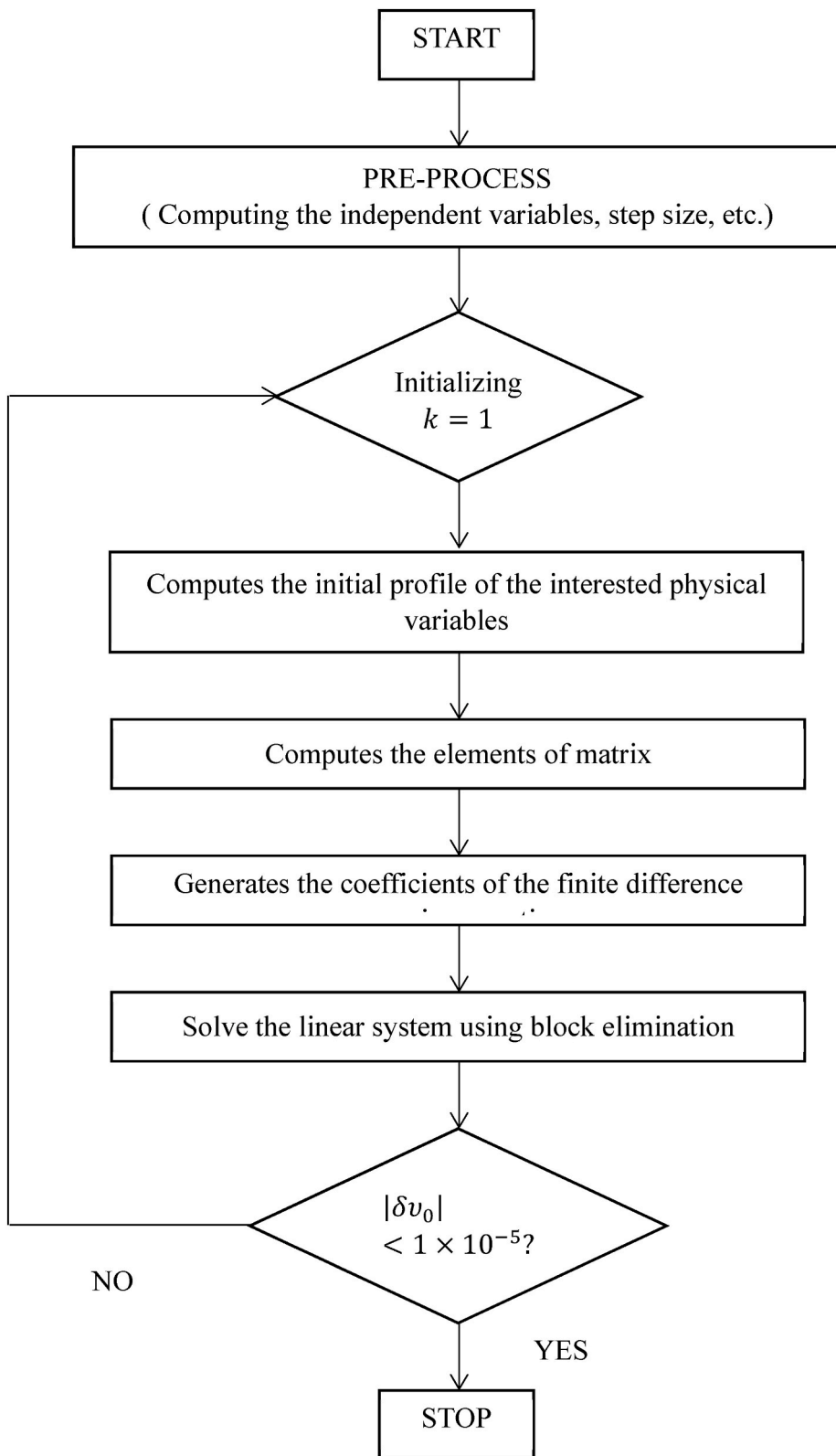
Fig. 2. Flow chart for the Keller box method.

iii. The application of the finite difference method leads to a set of nonlinear algebraic system equations. To linearize this system, Newton's approach is employed, introducing iterative values for the new dependent variables.

iv. The block tridiagonal factorization algorithm serves to deal with the matrix of the linear system. This scheme is specifically designed for block tri-diagonal matrices, which are matrices composed of blocks of matrices. The findings are obtained by employing the block-elimination method, commonly referred to as the Thomas algorithm, to solve the matrix equation. For more detailed information about this approach, further insights can be obtained from the works of Cebeci and Bradshaw [50] and Kamis et al. [51].

4. Results and discussion

The computation procedures have been performed for two hybrid ferro-nanofluids, $Fe_3O_4/CoFe_3O_4$ and $NiZnFe_2O_4/MnZnFe_2O_4$ in the combination of water-ethylene glycol as the conventional fluid in the current study. The effect of ferrohydrodynamic interaction (β), nanoparticles volume fraction (φ_2) and velocity slip (δ) on both hybrid ferro-nanofluids with different values of the dimensionless distance of the magnetic dipole (α) have been plotted and illustrated via graphs and tables. Through this study, the permanent parameters are $\varepsilon = 2.0, \chi = 0.01$ [8], and investigated parameters are in the range $0.5 \leq \alpha \geq 1.0$ [32], $1 \leq \beta \leq 5$ [19], $0.01 \leq \varphi_2 \geq 0.04$ [52], and $0.0 \leq \delta \leq 0.8$ [43].

4.1. Verification of the results

The validation of the results is presented in Table 5 by setting the parameters $Pr = 7$ and $\beta = \varphi_1 = \varphi_2 = 0$. The comparison yields excellent agreement with prior research [35–38,40]. The comparison shows that when the velocity slip escalates, the shear stress declines.

4.2. Dimensionless distance of the magnetic dipole (α)

The magnetic field generated by the magnetic bar has manipulated the flow of the hybrid ferro-nanofluids. The velocity ($f'(\eta)$) and temperature ($\theta(\eta)$) profiles of the fluid, as plotted in Figs. 3 and 4, respectively, are affected by the bar magnet's distance. It indicates that the greater the distance between the magnetic bar and the plate, the faster the fluid particles move along the stretching plate. According to the dimensionless equation (18) for α, it depicts that the growth of the α leads to an overall reduction in dynamic viscosity but an upsurge in hybrid ferro-nanofluids density. However, a change occurs when the sheet is stretched, and the fluid gets warm, causing the density of the hybrid ferro-nanofluids to decrease and the viscosity to increases. On the other hand, the nanoparticles encounter a weaker magnetic field as the magnetic bar moves further away from the plate. The hybrid ferro-nanofluids' magnetization drops. This drives the nanoparticles to speed up to battle the frictional force due to the increment in viscosity of the hybrid ferro-nanofluids. The figure clearly indicates that the momentum boundary layer turns thicker as the values of α increase. In a real-world application, the accuracy of transporting magnetic nanoparticles (cancer killers) to the cancer tumour can be improved by changing the intensity of the magnetic field by controlling the parameter α. This increases the chances of the magnetic nanoparticles accumulating in cancer cells, as reported in the experimental study of magnetic fluid hyperthermia written by Jordan et al. [53].

The reduction of the magnetic nanoparticles' magnetization also affected the heat contents in the hybrid nanoparticles. Magnetization saturation refers to the highest magnetic moment that the magnetic nanoparticles reach. When magnetization saturation is low, it implies that the nanoparticles respond poorly to the applied magnetic field. This slow reaction reduces the magnetic forces acting on the nanoparticles. As the intensity of the magnetic field decreases due to the growth of the parameter α, it reduces the rate of heat generation within the nanoparticles. Thereby, the temperature, as well as the thermal boundary layer, are diminished (see Fig. 4). In conclusion, the intensity of the magnetic field is important for ferromagnetic hybrid nanofluids to regulate the temperature of the hybrid magnetic nanoparticles. By controlling the parameter of α below the sheet, it is possible to control the heating or cooling effect on the magnetic nanoparticles, particularly in the application of targeted drug delivery, hyperthermia treatments, or temperature-sensitive materials (see the review paper published by Kumar and Muhammad [54]). In terms of comparative advantage, $NiZnFe_2O_4/MnZnFe_2O_4$ has a higher velocity profile as a result of stronger magnetic susceptibility (interaction between ferro nanoparticles with the magnetic fields from the magnetic dipole) in response to an applied magnetic field than $Fe_3O_4/CoFe_3O_4$ (see Fig. 3). However, it is detected that $Fe_3O_4/CoFe_3O_4$ is discovered to improve the temperature profile over $NiZnFe_2O_4/MnZnFe_2O_4$ due to a greater magnetization saturation, as illustrated in Fig. 4.

The velocity field for the effect of ferrohydrodynamic interaction β under different values of parameter α is designed in Fig. 5. The existence of the α (dimensionless distance from the origin to the center of the magnetic dipole), ε (Curie temperature), and β are

Table 5
Validation of the results for $f'(0)$.

δ	Andersson [35]	Wang [36]	Hayat et al. [37]	Noghrehabadi et al. [38]	Ibrahim et al. [40]	Present study
0.3	–	0.7010	–	0.7015	–	0.7010
0.5	0.5912	–	0.5912	0.5912	0.5912	0.5913
1.0	–	0.4300	–	0.4302	–	0.4305
2.0	0.2840	0.2840	0.2840	0.2840	0.2840	0.2842
5.0	0.1448	0.1450	0.1448	0.1448	0.1448	0.1451
20	0.0438	0.0438	0.0438	0.0438	0.0438	0.0439
50	0.0186	–	0.0186	–	0.0186	0.0187
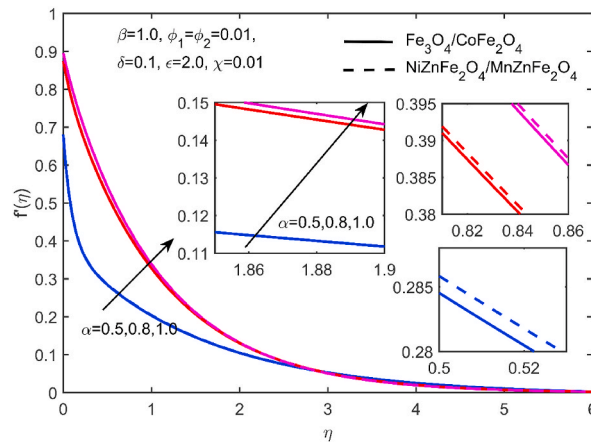
Fig. 3. Comparative analysis of hybrid ferro-nanofluids for various values of α on $f'(\eta)$.
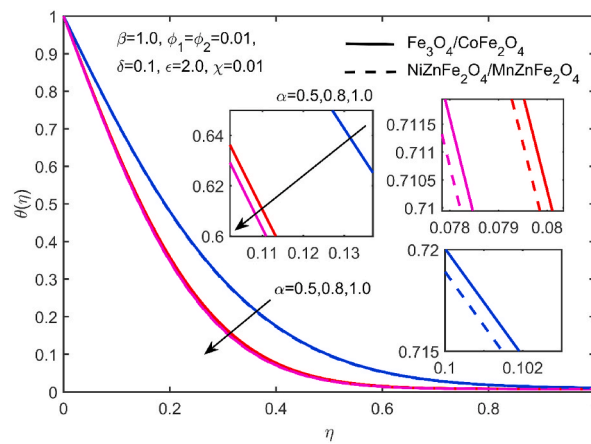
Fig. 4. Comparative analysis of hybrid ferro-nanofluids for various values of α on $\theta(\eta)$ 4.3 Ferrohydrodynamic interaction parameter (β).
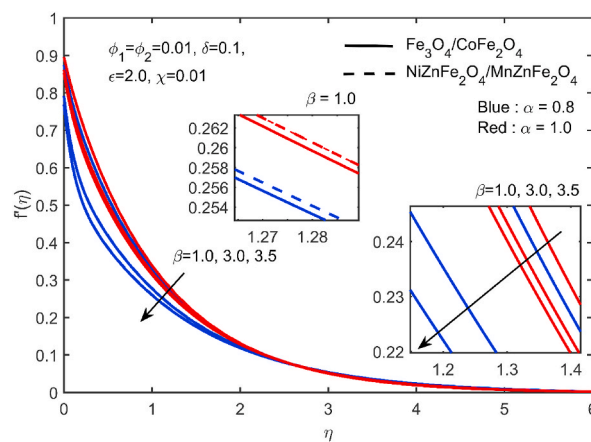
Fig. 5. Comparative analysis of hybrid ferro-nanofluids at two values of α for various values of β over $f'(\eta)$.

required to keep the impact of the ferromagnetic effect (FHD) on the boundary layer flow. It is observed that the velocity profile of the hybrid ferro-nanofluids shows a declination as the values of parameter β for both cases, $\alpha = 0.8$ and $\alpha = 1.0$ are enhanced. The FHD effect is improved as the values of β expand from 1 to 3. The applied magnetic field interacts with the magnetic nanoparticles in the hybrid ferro-nanofluids system, resulting in the saturation of the fluid and tending to escalate the development of magnetic chains or
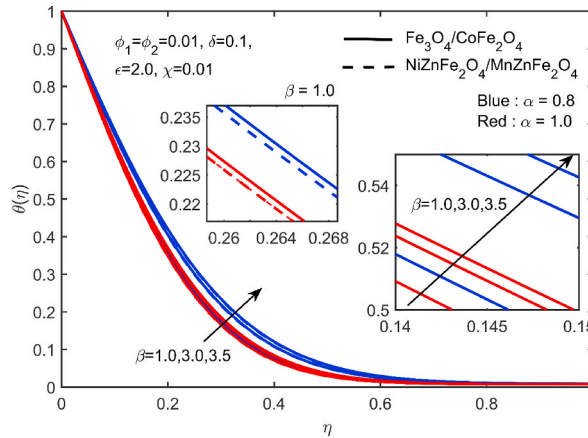
Fig. 6. Comparative analysis of hybrid ferro-nanofluids at two values of α for various values of β over $\theta(\eta)$ 4.4 Ferroparticles volume fraction (φ_2).

clusters. These chains or clusters changed the viscosity of the fluid, resulting in a rise in the hybrid ferro-nanofluids' effective viscosity. As a consequence, the fluid encounters more flow resistance. The magnetic chains created by the nanoparticles obstruct fluid motion, minimizing flow and dropping the overall velocity profile. As indicated in the preceding section, the distance of the magnetic dipole altered the behavior of the fluid by increasing the velocity field as the magnetic bar distanced itself from the sheet. Hence, Fig. 5 reveals that when the bar magnet is closer to the sheet with $\alpha = 0.8$, the velocity field declines fast, followed by parameter β with $\alpha = 1.0$. When ethylene glycol plus water is used as the base fluid, it is also seen that hybrid ferro-nanofluids, $Fe_3O_4/CoFe_3O_4$ rapidly reduces the velocity field of the ferromagnetic hybrid nanofluids.

The influence of β on the temperature field is addressed in Fig. 6. The hybrid ferro-nanofluids respond to the magnetic field more strongly as the parameter β rises. The nanoparticles in the hybrid ferro-nanofluids experience a force and begin to move when it is exposed to a magnetic field, causing fluid movement and convective heat transfer. The temperature of the hybrid ferro-nanofluids rises as a result of the nanoparticles' mobility, creating frictional heating. Hence, the temperature profile upsurges along with an escalation in the thermal boundary layer thickness. It is disclosed from Fig. 6 that an enhancement of the values for the parameter β prompts a change in the temperature profile of the hybrid ferro-nanofluids, $Fe_3O_4/CoFe_3O_4$ and $NiZnFe_2O_4/MnZnFe_2O_4$ at different distances from the magnetic dipole. In view of the high magnetization saturation of $Fe_3O_4/CoFe_3O_4$, more heat from the sheet is delivered to the ferromagnetic hybrid fluid of the nanoparticle during convection. In addition, the maximum magnetic field intensity at $\alpha = 0.8$ also boosts the heat content when the sheet is stretched. Because of the amplification of the temperature field against parameter β, the presence of $Fe_3O_4/CoFe_3O_4$ that pushes the magnetic bar closer to the sheet can be utilized to selectively heat and treat malignant cells in hyperthermia cancer therapy. This kind of localized and controlled heating has the potential to provide focused and efficient cancer therapy while causing minimal harm to healthy tissues.

Figs. 7 and 8 are plotted to analyze the influence of φ_2 on velocity and temperature fields, respectively. Remarkably, the velocity profile drops off as increases the concentration volume fraction for ferro nanoparticles. The momentum boundary layer evolves thinner as a result of the propagation of ferro nanoparticles near the sheet. The hybrid ferro-nanofluids become more viscous as a result of the addition of ferro nanoparticles due to the additional aggregation and clustering of the particles. Further, it impedes fluid movement by building up resistance and limiting the flow of the fluid. Decrementation of the magnetic dipole's distance significantly decays the
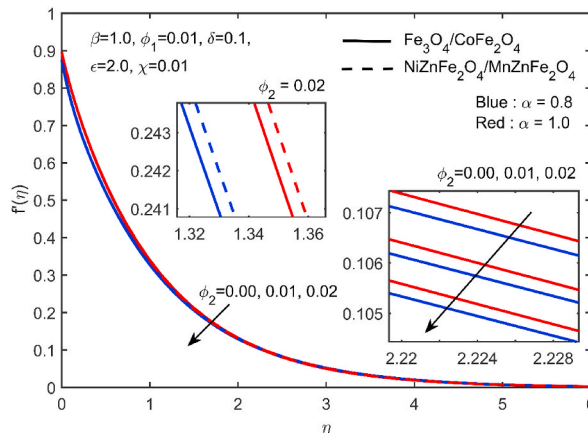
Fig. 7. Comparative analysis of hybrid ferro-nanofluids at two values of α for various values of φ_2 over $f'(\eta)$.
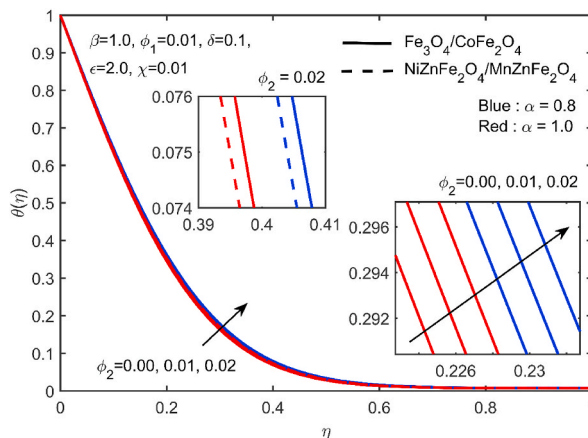
Fig. 8. Comparative analysis of hybrid ferro-nanofluids at two values of α for various values of φ_2 over $\theta(\eta)$ *4.5 Velocity slip (δ).*

velocity, as shown in Fig. 7 when the dimensionless α is set from 1.0 to 0.8. This indicates that the strength of the magnetic field produced by the magnetic bar does not balance the increment viscosity of the hybrid ferro-nanofluids as the parameter φ_2 raises. This is because it does not directly affect the molecular structure of the fluid or the intermolecular forces that cause viscosity. It is interesting to mention that when compared to $Fe_3O_4/CoFe_3O_4$, the hybrid ferro-nanofluids of $NiZnFe_2O_4/MnZnFe_2O_4$ move more quickly under the influence of the magnetic dipole. It means that the magnetic susceptibility is greater in hybrid ferro-nanofluids, $NiZnFe_2O_4/MnZnFe_2O_4$ flow than in $Fe_3O_4/CoFe_3O_4$ along the stretching sheet. Because of their enhanced magnetic susceptibility, $NiZnFe_2O_4/MnZnFe_2O_4$ nanoparticles respond more strongly to applied magnetic fields, resulting in more powerful magnetophoretic effects. Hence, the magnetophoretic force moves the nanoparticles faster within the fluid.

As shown in Fig. 8, the increase in ferro nanoparticle volume percentage has an impact on the temperature profile. The thermal boundary layer thickness increases by increasing the parameter of φ_2 with an accompanying rise in the temperature profile. The temperature and thermal boundary layer of $\alpha = 0.8$ is higher compared to $\alpha = 1.0$. It is obvious that when the magnetic bar moves near the sheet, the greater magnetic field allows the heat generated by the magnetic nanoparticles to be transmitted to the hybrid ferro-nanofluids and the neighboring sheet by conduction and convection. The outcome of φ_2 holds great importance in applications related to hyperthermia drug release, as asserted in an experimental investigation by Tabatabaei and Martel [55]. In this study, the researchers could anticipate the requisite concentration of magnetic nanoparticles for achieving the desired temperature, thus enhancing the optimization of the cancer therapy procedure. Furthermore, $Fe_3O_4/CoFe_3O_4$ has a higher temperature field than $NiZnFe_2O_4/MnZnFe_2O_4$. As the ferro nanoparticles volume fraction for $CoFe_3O_4$ goes up, so does the saturation magnetization of the ferromagnetic hybrid nanofluid is increased. Physically, $CoFe_3O_4$ has a higher saturation magnetization and heat transfer than other ferro nanoparticles, even where there is no external magnetic field [47,56]. It is interesting to mention that $CoFe_3O_4$ shows ferromagnetic behavior and also excellent chemical stability, making it a hard magnetic material with promising candidates for medical applications like hyperthermia cancer therapy [57]. Thus, the ferro hybrid-nanofluids, $Fe_3O_4/CoFe_3O_4$ may have higher heat generation efficiency due to their composition and magnetic properties, thereby increasing the saturation magnetization when subjected to an external magnetic field. As a result of the high magnetism and excellent heat transmission of $Fe_3O_4/CoFe_3O_4$, the application of
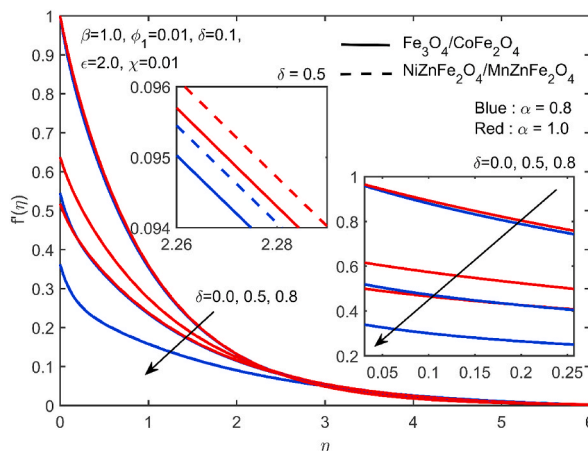
Fig. 9. Comparative analysis of hybrid ferro-nanofluids at two values of α for various values of δ over $f^{'}(\eta)$.
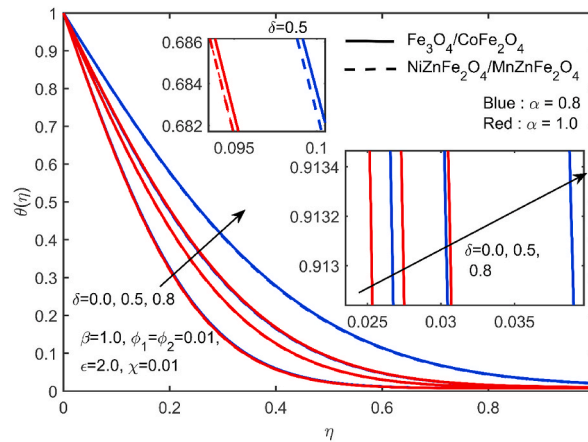
Fig. 10. Comparative analysis of hybrid ferro-nanofluids at two values of α for various values of δ over $\theta(\eta)$ 4.5 Local skin friction and Nusselt number.

such a hybrid nanoparticle in hyperthermia treatment for targeting cancer tissue may be more effective [58,59].

Fig. 9 depicts the comparative analysis of hybrid ferro-nanofluids at two values of α for various values of δ over $f'(\eta)$. It is shown that the velocity profile declines when the velocity slip increases. When $\delta = 0$ refers to the no-slip case, then the velocity is equal to one based on the boundary condition (17). The term velocity slip or slip condition case as $\delta \neq 0$ is the relative motion between the fluid and the solid surface. It occurs when the fluid velocity at the surface is not parallel to the surface velocity. The reduction of the ferro nanoparticles' movement along the stretching sheet happens due to the enhancement of the lubrication and slippage at the surface as implied by the larger value of δ. According to the dimensionless equation (18), the growth of δ causes the factor of slip velocity to increase however reduces the kinematic viscosity, thereby vanishing the momentum boundary layer thickness. It is also revealed that the velocity of the fluid under the no-slip condition has a higher velocity near the surface compared to the slip condition. Besides, the difference in the intensity of the magnetic field when altering the value of α also affects the characteristics of the hybrid ferro-nanofluids during the stretching sheet. The fast reduction of the $f'(\eta)$ is detected when $\alpha = 1.0$. It indicates that the strongest magnetic field intensity is vital in controlling the movement of the magnetic nanoparticles to move faster at the targeted cell or organ during cancer treatment. The velocity field is marginally lower for the $Fe_3O_4/CoFe_3O_4$ than for the $NiZnFe_2O_4/MnZnFe_2O_4$ due to the higher magnetic properties in $Fe_3O_4/CoFe_3O_4$, which have a stronger interaction effect with the non-electrically conductive ferro-magnetic hybrid nanofluid.

Fig. 10 signifies the influence of temperature distribution for increasing values of δ. The velocity slip adjusts the behavior of the flow by carrying away the heat from the surface, thereby upsurging the temperature difference between the hybrid ferro-nanofluids and the sheet. Specifically, a rise in the velocity slip may boost the thermal boundary layer. It is evident that the velocity slip enhances the convective heat transfer between the nanoparticles and the surrounding fluid. It can also be seen in Fig. 10 that when the velocity slip parameter is ignored ($\delta = 0$), the thermal boundary layer is closer to the sheet than $\delta \neq 0$. Consequently, considering the slip velocity is critical for determining the percentage of internal heat content in the hybrid ferro-nanofluids in order to optimize the heating and cooling processes of a system. The highest temperature is achieved at the maximum magnetic intensity ($\alpha = 0.8$) with the hard magnetic nanoparticles, $Fe_3O_4/CoFe_3O_4$ is used, and this happens concurrently with a rise in the parameter of δ. This is due to the fact that one of the properties of hard magnetic is hysteresis or a material's resistance to changes in its magnetism. When subjected to an alternating magnetic field, the nanoparticles quickly modify their magnetic orientation, which results in energy being wasted as heat. In addition, the slip velocity impact causes a quick rise in the hysteresis process in the nanoparticles because the slip speed changes, affecting the heat content of the ferromagnetic hybrid nanofluids.

The influence of parameter α on local skin friction $C_f Re_x^{\frac{1}{2}}$ and Nusselt number $Nu_x Re_x^{-\frac{1}{2}}$ are tabulated in Table 6. It is seen that the expansion of the distance magnetic bar from the sheet at $x-$ axis reduces the values of $C_f Re_x^{\frac{1}{2}}$ for both hybrid ferro-nanofluids, $Fe_3O_4/CoFe_3O_4$ and $NiZnFe_2O_4/MnZnFe_2O_4$. This decrement is attributed to the weaker interaction between the magnetic field and the magnetic nanoparticles, resulting in a decrease in the wall shear stress of the hybrid ferro-nanofluids as it flows over the stretching sheet. It is evident from Table 4 that the fast reduction in wall shear stress is observed for $Fe_3O_4/CoFe_3O_4$ due to a lower viscosity against to $NiZnFe_2O_4/MnZnFe_2O_4$. A lower viscosity means smoother flow and less resistance to shear, which leads to an instantaneous decline in $C_f Re_x^{\frac{1}{2}}$. $Nu_x Re_x^{-\frac{1}{2}}$ improves when the parameter α is increased. The magnetic field impact on fluid flow and heat transfer diminishes as the separation between the magnetic bar and the plate rises. As an outcome, convective heat transfer processes may predominate over conductive heat transfer. The lower heat transfer rate is observed for $Fe_3O_4/CoFe_3O_4$ compared to $NiZnFe_2O_4/MnZnFe_2O_4$.

The effect of the parameter β is highlighted in Table 7 for both $C_f Re_x^{\frac{1}{2}}$ and $Nu_x Re_x^{-\frac{1}{2}}$ as parameter α has been set to 0.8 and 1.0 together for hybrid ferro nanofluids, $Fe_3O_4/CoFe_3O_4$ and $NiZnFe_2O_4/MnZnFe_2O_4$, respectively, along the stretching sheet. The findings showed that in both situations, $C_f Re_x^{\frac{1}{2}}$ increases with the values of β. However, $Nu_x Re_x^{-\frac{1}{2}}$ behaves oppositely for the upsurging

Table 6

Comparative analysis of hybrid ferro-nanofluids various values of parameters α over $C_f Re_x^{\frac{1}{2}}$ and $Nu_x Re_x^{-\frac{1}{2}}$.

Parameter	Fe$_3$O$_4$/CoFe$_3$O$_4$		NiZnFe$_2$O$_4$/MnZnFe$_2$O$_4$	
α	$-C_f Re_x^{\frac{1}{2}}$	$-Nu_x Re_x^{-\frac{1}{2}}$	$-C_f Re_x^{\frac{1}{2}}$	$-Nu_x Re_x^{-\frac{1}{2}}$
0.5	3.1952	2.1662	3.1904	2.1784
0.8	1.2572	3.4683	1.2548	3.4801
1.0	1.0449	3.9406	1.0427	3.6573

Table 7

Comparative analysis of hybrid ferro-nanofluids at two values of α for various values of parameters β, φ_2, and δ over $C_f Re_x^{\frac{1}{2}}$ and $Nu_x Re_x^{-\frac{1}{2}}$.

Investigated parameters			$\alpha = 0.8$				$\alpha = 1.0$			
β	φ_2	δ	Fe$_3$O$_4$/CoFe$_3$O$_4$		NiZnFe$_2$O$_4$/MnZnFe$_2$O$_4$		Fe$_3$O$_4$/CoFe$_3$O$_4$		NiZnFe$_2$O$_4$/MnZnFe$_2$O$_4$	
			$-C_f Re_x^{\frac{1}{2}}$	$-Nu_x Re_x^{-\frac{1}{2}}$	$-C_f Re_x^{\frac{1}{2}}$	$-Nu_x Re_x^{-\frac{1}{2}}$	$-C_f Re_x^{\frac{1}{2}}$	$-Nu_x Re_x^{-\frac{1}{2}}$	$-C_f Re_x^{\frac{1}{2}}$	$-Nu_x Re_x^{-\frac{1}{2}}$
1.0			1.2572	3.4683	1.2548	3.4801	1.0449	3.6454	1.0427	3.6573
3.0			2.0841	2.8957	2.0805	2.9076	1.3858	3.3817	1.3832	3.3936
3.5			2.3139	2.7521	2.3100	2.7606	1.4741	3.3187	1.4714	3.3306
	0.00		1.2623	3.4914	1.0450	3.6707	1.2609	3.4952	1.0437	3.6745
	0.01		1.2572	3.4683	1.0449	3.6454	1.2548	3.4801	1.0427	3.6573
	0.02		1.2517	3.4421	1.0442	3.6171	1.2484	3.4618	1.0413	3.6368
		0.0	1.4224	3.7271	1.1910	3.8636	1.1419	3.7391	1.1889	3.8756
		0.5	0.9108	2.6822	0.9096	2.6821	0.7261	3.0401	0.8492	3.0511
		0.8	0.7840	2.0849	0.7971	2.0914	0.6037	2.7146	0.7250	2.9842

parameter β. The rise in the intensity of the magnetic field for $\alpha = 0.8$ has enhanced the wall shear stress because $C_f Re_x^{\frac{1}{2}}$ for $\alpha = 0.8$ is greater than $\alpha = 1.0$. In terms of $Nu_x Re_x^{-\frac{1}{2}}$, when the dimensionless distance of the magnetic dipole is changed to a high value, the heat transfer rate escalates faster. Hybrid ferro-nanofluids, Fe$_3$O$_4$/CoFe$_3$O$_4$ demonstrate higher values for both physical quantities due to higher saturation magnetization than the magnetic nanoparticles, NiZnFe$_2$O$_4$/MnZnFe$_2$O$_4$.

Table 7 reveals the numerical values of physical quantities, $C_f Re_x^{\frac{1}{2}}$ and $Nu_x Re_x^{-\frac{1}{2}}$ for various φ_2. From the table, it is clearly seen that $C_f Re_x^{\frac{1}{2}}$ diminishes for Fe$_3$O$_4$/CoFe$_3$O$_4$ and NiZnFe$_2$O$_4$/MnZnFe$_2$O$_4$. Muhammad et al. [13] also claimed the same behavior of the wall shear stress for NiZnFe$_2$O$_4$/MnZnFe$_2$O$_4$. The upsurge of the viscosity in the magnetic nanoparticle alters the hybrid ferro-nanofluids flow by decaying the shear stress. However, the maximum shear stress is observed for Fe$_3$O$_4$/CoFe$_3$O$_4$ when $\alpha = 0.8$. $Nu_x Re_x^{-\frac{1}{2}}$ of the hybrid ferro-nanofluids decays with the growth of φ_2 for all cases. In general, at $\alpha = 1.0$, the heat transfer rate is higher than $\alpha = 0.8$ due to the reduction in the intensity of the magnetic field. The higher saturation magnetization in the magnetic materials of Fe$_3$O$_4$/CoFe$_3$O$_4$ demonstrates a lower reduction of the $Nu_x Re_x^{-\frac{1}{2}}$.

Furthermore, the effect of the slip velocity is also presented in Table 7. The $C_f Re_x^{\frac{1}{2}}$ and $Nu_x Re_x^{-\frac{1}{2}}$ decline abruptly for a larger number of δ. In general, when the velocity at the sheet is modified by the transverse velocity gradient, which is the derivative of the tangential slip velocity normal to the wall surface, the shear stress and heat transfer rate disappears. Another significant point that can be concluded from Table 5, there is less friction force on the sheet when the magnetic dipole moves away from the sheet ($\alpha = 1.0$). Thus, the magnetic dipole at $\alpha = 0.8$ improves the deformation of the hybrid ferro-nanofluids by enhancing the parameter δ. The convective heat transfer is upsurged in the magnetic nanoparticles, Fe$_3$O$_4$/CoFe$_3$O$_4$ due to the higher values of $Nu_x Re_x^{-\frac{1}{2}}$. However, the conductive heat transfer is found to increase more than the convective heat transfer for NiZnFe$_2$O$_4$/MnZnFe$_2$O$_4$ due to the decrementation in the values of the Nusselt number.

5. Conclusion

This study aimed to investigate the effects of hybrid ferro-nanofluids, specifically Fe$_3$O$_4$ $-$ CoFe$_2$O$_4$ and NiZnFe$_2$O$_4$/MnZnFe$_2$O$_4$ with a magnetic dipole on the heat transfer characteristics of a flowing mixture of water-ethylene glycol over a slip stretching sheet. To accomplish this, we utilized a finite difference method, which is called the Keller box method, in MATLAB software to solve the governing equations. By systematically altering parameters such as the strength of the magnetic dipole, ferrohydrodynamic interaction, volume fraction of ferro nanoparticles, and slip velocity, we investigated their effects on important aspects of the system, including the profile of velocity, temperature, skin friction coefficient, and rate of heat transfer. The main findings obtained from our investigation are outlined below:

   i. The velocity profile demonstrates an increasing trend with an increase in α, indicating a higher flow velocity. However, a contrasting pattern is observed for the temperature profile, where it decreases with the same increase in α,

   ii. The temperature profile rises due to the growth of parameters β and δ,

  iii. The boost of parameters β and δ in both ferro hybrid nanofluids cut off the particles' speed movement,

  iv. The augmentation of nanoparticles volume fraction, specifically $CoFe_2O_4$ and $MnZnFe_2O_4$ leads to the diminishing of the velocity profile, however, amplifies the temperature profile due to the elevated values of viscosity and thermal conductivity.

   v. The fast reduction has happened in the velocity profile for $Fe_3O_4 - CoFe_2O_4$ at $\alpha = 0.8$,

  vi. The heat content in $Fe_3O_4 - CoFe_2O_4$ is higher than $NiZnFe_2O_4/MnZnFe_2O_4$ when a stronger magnetic field intensity is applied,

 vii. When α varies from 0.5 to 1.0, the decrement of local skin friction for $Fe_3O_4 - CoFe_2O_4$ and $NiZnFe_2O_4/MnZnFe_2O_4$ are 67.30 % and 67.41 %, respectively,

viii. When α varies from 0.5 to 1.0, the increment of heat transfer rate for $Fe_3O_4 - CoFe_2O_4$ and $NiZnFe_2O_4/MnZnFe_2O_4$ are 81.91 % and 67.81 %, respectively,

  ix. Almost 2.33 % of the difference in local skin friction for $Fe_3O_4 - CoFe_2O_4$ when changing the velocity slip at $\alpha = 0.8$,

   x. The findings from this research are highly relevant for heat transfer systems, including the cooling and heating process of cancer treatment and MRI in biomedical engineering applications.

  xi. In future investigations, the present study could be expanded by incorporating non-Newtonian fluids such as blood (Casson fluid [60]) or by taking into account second-order velocity slip [61] or the size of the nanoparticles [62].

Declaration of competing interest

The authors declare that they have no known competing financial interests or personal relationships that could have appeared to influence the work reported in this paper.

Data availability

No data was used for the research described in the article.

Acknowledgment

References

[1] S. Papell, Low Viscosity Magnetic Fluid Obtained by the Colloidal Suspension of Magnetic Particles Patent, 1965.

[2] R. Rosensweig, Ferrohydrodynamics, Cambridge Univ. Press, Cambridge, 1985, p. 344.

[3] J. Popplewell, et al., Thermal conductivity measurements on ferrofluids, Colloid Polym. Sci. 260 (1982) 333–338.

[4] B.A. Finlayson, Convective instability of ferromagnetic fluids, J. Fluid Mech. 40 (4) (1970) 753–767.

[5] N.S. Mousavi, S. Kumar, S.D. Khapli, PROPERTIES OF FERROFLUIDS, 1984.

[6] K. Raj, R. Boulton, Ferrofluids—properties and applications, Mater. Des. 8 (4) (1987) 233–236.

[7] M. Sheikholeslami, D.D. Ganji, Ferrohydrodynamic and magnetohydrodynamic effects on ferrofluid flow and convective heat transfer, Energy 75 (2014) 400–410.

[8] H. Andersson, O. Valnes, Flow of a heated ferrofluid over a stretching sheet in the presence of a magnetic dipole, Acta Mech. 128 (1) (1998) 39–47.

[9] M. Sheikholeslami, D.D. Ganji, M.M. Rashidi, Ferrofluid flow and heat transfer in a semi annulus enclosure in the presence of magnetic source considering thermal radiation, J. Taiwan Inst. Chem. Eng. 47 (2015) 6–17.

[10] S.U. Choi, J.A. Eastman, Enhancing Thermal Conductivity of Fluids with Nanoparticles, Argonne National Lab.(ANL), Argonne, IL (United States), 1995.

[11] S. Angayarkanni, J. Philip, Review on thermal properties of nanofluids: recent developments, Adv. Colloid Interface Sci. 225 (2015) 146–176.

[12] N. Muhammad, S. Nadeem, Ferrite nanoparticles Ni-ZnFe 2 O 4, Mn-ZnFe 2 O 4 and Fe 2 O 4 in the flow of ferromagnetic nanofluid, The Eur. Phys. J. Plus 132 (2017) 1–12.

[13] N. Muhammad, S. Nadeem, M. Mustafa, Analysis of ferrite nanoparticles in the flow of ferromagnetic nanofluid, PLoS One 13 (1) (2018), e0188460.

[14] S. Nadeem, S. Ahmad, N. Muhammad, Analysis of ferrite nanoparticles in liquid, Pramana 94 (2020) 1–9.

[15] A.S. Negi, B. Kumar, Nano-ferrofluid (Mn–Zn, CoFe2O4, Fe3O4) flow in a permeable channel with induced magnetic field, Waves Random Complex Media (2023) 1–28.

[16] S. Yasin, et al., MHD free convection boundary layer flow near the lower stagnation point flow of a horizontal circular cylinder in ferrofluid, in: IOP Conference Series: Materials Science and Engineering, IOP Publishing, 2020.

[17] M.K.A. Mohamed, F.N. Abas, M.Z. Salleh, MHD boundary layer flow over a permeable flat plate in a ferrofluid with thermal radiation effect, in: Journal of Physics: Conference Series, IOP Publishing, 2019.

[18] R.N. Kumar, et al., Impact of magnetic dipole on ferromagnetic hybrid nanofluid flow over a stretching cylinder, Phys. Scripta 96 (4) (2021), 045215.

[19] H. Tahir, et al., Hybridized two phase ferromagnetic nanofluid with NiZnFe2O4 and MnZnFe2O4, Ain Shams Eng. J. 12 (3) (2021) 3063–3070.

[20] M. Ijaz Khan, et al., Marangoni convective flow of hybrid nanofluid (MnZnFe2O4-NiZnFe2O4-H2O) with Darcy Forchheimer medium, Ain Shams Eng. J. 12 (4) (2021) 3931–3938.

[21] J. Yang, et al., Hydrodynamics and ferrite nanoparticles in hybrid nanofluid, Int. Commun. Heat Mass Tran. 118 (2020), 104883.

[22] K. Anantha Kumar, et al., Effect of electromagnetic induction on the heat transmission in engine oil-based hybrid nano and ferrofluids: a nanotechnology application, Proc. IME E J. Process Mech. Eng. (2022), 09544089221139569.

[23] N.S. Anuar, N. Bachok, I. Pop, Influence of MHD hybrid ferrofluid flow on exponentially stretching/shrinking surface with heat source/sink under stagnation point region, Mathematics 9 (22) (2021) 2932.

[24] G. Ramesh, et al., Thermodynamics examination of Fe 3 O 4-CoFe 2 O 4/water+ EG nanofluid in a heated plate: crosswise and stream-wise aspects, Arabian J. Sci. Eng. (2021) 1–10.

[25] S. Zainodin, et al., Effects of higher order chemical reaction and slip conditions on mixed convection hybrid ferrofluid flow in a Darcy porous medium, Alex. Eng. J. 68 (2023) 111–126.

[26] I. Waini, et al., Unsteady magnetohydrodynamics (MHD) flow of hybrid ferrofluid due to a rotating disk, Mathematics 10 (10) (2022) 1658.

[27] S. Saranya, L. Baranyi, Q.M. Al-Mdallal, Free convection flow of hybrid ferrofluid past a heated spinning cone, Therm. Sci. Eng. Prog. 32 (2022), 101335.

[28] K. Anantha Kumar, et al., Effect of irregular heat source/sink on the radiative thin film flow of MHD hybrid ferrofluid, J. Therm. Anal. Calorim. 139 (2020) 2145–2153.

[29] B.D. Cullity, C.D. Graham, Introduction to Magnetic Materials, John Wiley & Sons, 2011.

[30] K. Seleznyova, M. Strugatsky, J. Kliava, Modelling the magnetic dipole, Eur. J. Phys. 37 (2) (2016), 025203.

[31] J.L. Neuringer, R.E. Rosensweig, Ferrohydrodynamics, Phys. Fluid. 7 (12) (1964) 1927–1937.

[32] T. Yasmeen, et al., Ferrofluid flow by a stretched surface in the presence of magnetic dipole and homogeneous-heterogeneous reactions, J. Mol. Liq. 223 (2016) 1000–1005.

[33] A. Almaneea, Thermal analysis for ferromagnetic fluid with hybrid nano-metallic structures in the presence of Forchheirmer porous medium subjected to a magnetic dipole, Case Stud. Therm. Eng. 26 (2021), 100961.

[34] C. Shu-Bo, et al., Thermophoretic particle deposition in the flow of dual stratified Casson fluid with magnetic dipole and generalized Fourier's and Fick's laws, Case Stud. Therm. Eng. 26 (2021), 101186.

[35] H.I. Andersson, Slip flow past a stretching surface, Acta Mech. 158 (1–2) (2002) 121–125.

[36] C. Wang, Flow due to a stretching boundary with partial slip—an exact solution of the Navier–Stokes equations, Chem. Eng. Sci. 57 (17) (2002) 3745–3747.

[37] T. Hayat, M. Qasim, S. Mesloub, MHD flow and heat transfer over permeable stretching sheet with slip conditions, Int. J. Numer. Methods Fluid. 66 (8) (2011) 963–975.

[38] A. Noghrehabadi, R. Pourrajab, M. Ghalambaz, Effect of partial slip boundary condition on the flow and heat transfer of nanofluids past stretching sheet prescribed constant wall temperature, Int. J. Therm. Sci. 54 (2012) 253–261.

[39] A. Zeeshan, et al., Mixed convection flow and heat transfer in ferromagnetic fluid over a stretching sheet with partial slip effects, Therm. Sci. 22 (6 Part A) (2018) 2515–2526.

[40] W. Ibrahim, B. Shankar, MHD boundary layer flow and heat transfer of a nanofluid past a permeable stretching sheet with velocity, thermal and solutal slip boundary conditions, Comput. Fluid 75 (2013) 1–10.

[41] A. Majeed, A. Zeeshan, T. Hayat, Analysis of magnetic properties of nanoparticles due to applied magnetic dipole in aqueous medium with momentum slip condition, Neural Comput. Appl. 31 (2019) 189–197.

[42] Z. Iqbal, B. Ahmad, E.N. Maraj, A numerical study of ferrofluid (fe 3 o 4) in the presence of a magnetic dipole inspired by slip and viscous dissipation effects submerged in a porous medium, J. Porous Media 22 (1) (2019).

[43] A. Majeed, et al., Heat transfer in magnetite (Fe 3 O 4) nanoparticles suspended in conventional fluids: refrigerant-134A (C 2 H 2 F 4), kerosene (C 10 H 22), and water (H 2 O) under the impact of dipole, Heat Tran. Res. 51 (3) (2020).

[44] T.S. Kumar, Hybrid nanofluid slip flow and heat transfer over a stretching surface, Part. Differ. Equ. Appl. Math. 4 (2021), 100070.

[45] M. Akbari, et al., An experimental study on rheological behavior of ethylene glycol based nanofluid: proposing a new correlation as a function of silica concentration and temperature, J. Mol. Liq. 233 (2017) 352–357.

[46] A. Elsayed, et al., Synthesis and properties of polyaniline/ferrites nanocomposites, Int. J. Electrochem. Sci. 6 (1) (2011) 206–221.

[47] M. Padervand, et al., An experimental and theoretical study on the structure and photoactivity of XFe 2 O 4 (X= Mn, Fe, Ni, Co, and Zn) structures, Russ. J. Phys. Chem. A 88 (2014) 2451–2461.

[48] K.G. Kumar, et al., A novel approach for investigation of heat transfer enhancement with ferromagnetic hybrid nanofluid by considering solar radiation, Microsyst. Technol. 27 (1) (2021) 97–104.

[49] T. Chen, A. Mucoglu, Analysis of mixed forced and free convection about a sphere, Int. J. Heat Mass Tran. 20 (8) (1977) 867–875.

[50] T. Cebeci, P. Bradshaw, in: s (Ed.), Physical and Computational Aspects of Convective Heat Transfer, Springer, New York, 1988.

[51] N.I. Kamis, et al., Numerical simulation of convection hybrid ferrofluid with magnetic dipole effect on an inclined stretching sheet, Alex. Eng. J. 76 (2023) 19–33.

[52] H.C. Brinkman, The viscosity of concentrated suspensions and solutions, J. Chem. Phys. 20 (4) (1952), 571-571.

[53] A. Jordan, et al., Presentation of a new magnetic field therapy system for the treatment of human solid tumors with magnetic fluid hyperthermia, J. Magn. Magn. Mater. 225 (1–2) (2001) 118–126.

[54] C.S. Kumar, F. Mohammad, Magnetic nanomaterials for hyperthermia-based therapy and controlled drug delivery, Adv. Drug Deliv. Rev. 63 (9) (2011) 789–808.

[55] S.N. Tabatabaei, S. Martel, The concentration effect of magnetic iron oxide nanoparticles on temperature change for hyperthermic drug release applications via AC magnetic field, in: In Fifth Int. Conf. On Microtechnologies, Medicine and Biology (MMB), Citeseer, 2009.

[56] M. Dinarvand, et al., Experimental investigation and performance comparison of Fe3O4/water and CoFe2O4/water ferrofluids in presence of a magnetic field in a cooling system, J. Taiwan Inst. Chem. Eng. 148 (2023), 104927.

[57] S. Amiri, H. Shokrollahi, The role of cobalt ferrite magnetic nanoparticles in medical science, Mater. Sci. Eng. C 33 (1) (2013) 1–8.

[58] I. Sharifi, H. Shokrollahi, S. Amiri, Ferrite-based magnetic nanofluids used in hyperthermia applications, J. Magn. Magn Mater. 324 (6) (2012) 903–915.

[59] V. Vijayakanth, K. Chintagumpala, A review on an effect of dispersant type and medium viscosity on magnetic hyperthermia of nanoparticles, Polym. Bull. 80 (5) (2023) 4737–4781.

[60] M. Murtaza, et al., Numerical simulation of slip flow and heat transfer of biomagnetic fluid over a stretching sheet in the presence of a magnetic dipole with temperature dependent viscosity, Contemp. Math. (2023) 320–334.

[61] M. Hussain, et al., Nonsimilar forced convection analysis of magneto nanofluid (CNTs+ Water) flow in Darcy–Forchheimer porous media subjected to thermal radiations and heat generation/absorption, Waves Random Complex Media (2022) 1–14.

[62] A. Zaraki, et al., Theoretical analysis of natural convection boundary layer heat and mass transfer of nanofluids: effects of size, shape and type of nanoparticles, type of base fluid and working temperature, Adv. Powder Technol. 26 (3) (2015) 935–946.